Electronic Supplementary Information

N-heteroaromatic fused-ring cyanides extended as redox polymers for high rate capability aqueous zinc-ion battery†

*Xinlei Wang, Jie Zhou, Zhipeng Li and Weihua Tang**

Experimental section

Chemicals and materials

Chemicals including hexaketocyclohexane octahydrate ($C_6O_6 \cdot 8H_2O$), 4,5-diaminophthalonitrile, diaminomaleonitrile (DMAN), acetic acid (AcOH) and anhydrous zinc chloride ($ZnCl_2$) were purchased from Energy Chemical Co. Ltd. $ZnSO_4 \cdot 7H_2O$ (99%) was purchased from Aladdin. All chemicals were used directly without further purification

Synthesis of PHATN-t and PHAT-t

PHATN-t was synthesized via two-step procedure, which refers to relevant literature.[S1, S2] For PHATN-t, C_6O_6 (1.9 mmol, 0.6 g, 1 eq.), 4,5-diaminophthalonitrile (7.6 mmol, 1.2 g, 4 eq.) and AcOH (150 mL) were added into a two-neck round-bottom flask, followed by vigorous stirring at 115 °C for 48 h under nitrogen flow. After cooling to room temperature, the mixture was poured into water (200 mL) and filtered. The residue was washed with AcOH, ethyl alcohol, deionized water and acetone for several times in sequence. The obtained black solid was dried overnight at 60°C in vacuum to afford HATN-6CN (815 mg, 80.4% yield). Secondly, HATN-6CN (0.93 mmol, 500 mg, 1 eq.) and $ZnCl_2$ (9.3 mmol, 1.26 g, 10 eq.) were vacuum encapsulated in robust glass tube and then heated at 400 °C for 48 h. After breaking the glass tube, the obtained black solid was ground to powder and then added into hydrochloric acid (1 M, 100 mL) for overnight stirring. The black powder was filtered and washed with AcOH, ethanol, deionized water and acetone for several times. PHATN-t was then obtained after drying at 60°C in vacuum overnight (442 mg, 88.4% yield).

Refers to preparation of HATN-6CN and PHATN-t, the synthesis of HAT-6CN and PHAT-t follows a similar route. Specifically, C_6O_6 (1.9 mmol, 0.6 g, 1 eq.), DMAN (7.6 mmol, 0.83 g, 4 eq.) and AcOH (120 mL) were added into a two-neck round-bottom flask, followed by vigorous stirring at 115 °C for 48 h under nitrogen flow. After cooling to room temperature, the mixture was poured into water (200 mL) and filtered. The residue was washed with AcOH,

ethyl alcohol, deionized water and acetone for several times in sequence. The obtained black solid was dried overnight at 60°C in vacuum to afford HAT-6CN (548 mg, 74.3% yield). Secondly, HAT-6CN (1.3 mmol, 500 mg, 1 eq.) and $ZnCl_2$ (13 mmol, 1.77 g, 10 eq.) were vacuum encapsulated in robust glass tube and then heated at 400 °C for 48 h. After breaking the glass tube, the obtained black solid was ground to powder and then added into hydrochloric acid (1 M, 100 mL) for overnight stirring. The black powder was filtered and washed with AcOH, ethanol, deionized water and acetone for several times. PHAT-t was then obtained after drying at 60°C in vacuum overnight (431 mg, 86.2% yield).

Preparation of electrodes

The polymer powders of PHATN-t or PHAT-t, acetylene carbon, and polytetrafluoroethylene binder were mixed to prepare a slurry with mass ratio of 7:2:1. The slurry was coated onto pieces of carbon clothes and then dried in vacuum at 60 °C. Finally, these electrodes were cut as round pieces (diameter: 15 mm) with an average mass loading of 3 mg cm^{-2}.

Fabrication of aqueous zinc batteries

The ZIB performance based on PHATN-t or PHAT-t cathode was tested in CR2032-type coin cells, which were fabricated in ambient atmosphere with approximately 100 μL of 2 M $ZnSO_4$ aqueous electrolyte. Zinc anode (diameter: 15 mm; thickness: 0.5 mm) and PHATN-t or PHAT-t cathodes were separated by glass fiber separators (Whatman, GF/B).

Characterization and theoretical calculation

Field-emission scanning electron microscope (FE-SEM) images were recorded from J Hitachi S-4800 at an accelerating voltage of 3 kV. ^{13}C NMR spectra were collected on a Bruker ADVANCE 500 MHz spectrometer with trimethylsilane (TMS) as the internal reference. Solid state ^{13}C cross-polarization magic angle spinning nuclear magnetic resonance (CP/MAS NMR) spectra were collected on a Bruker AVANCE NEO 400 WB spectrometer (Bruker BioSpin AG, Fällanden, Switzerland) spectrometer. X-ray diffraction (XRD) patterns were recorded from Bruker D8 Advance Diffractometer. X-ray photoelectron spectroscopy (XPS) analysis was carried out on a Thermo ESCALAB 250 X-ray photoelectron spectrometer. Raman spectra were recorded on a RM 2000 microscopic confocal Raman spectrometer employing a 514 nm laser beam. The Fourier transform infrared (FT-IR) spectra were recorded from ThermoFisher Nicolet iS-10. The pore volume and specific surface area were measured by Brunauer-Emmet-Teller (BET) surface analyzer (Micromeritics, ASAP 2020).

Theoretical simulation and calculation were based on DFT with the B3LYP/6-31G (d,p) basis set. The solvation effect using implicit solvation model (SMD) for a precise simulation of the experimental conditions in aqueous solution is also considered in the optimization. After the molecules were optimized and calculated by DFT, the files of molecular calculation were further used to calculate electrostatic potential (ESP) by a software of GaussView 5.0. Molecular surface electrostatic potential was mapped by a software of VMD. Van der Waals surface is defined by electron density level of 0.001 e $Bohr^{-3}$.

Electrochemical Measurement

All electrochemical measurements were conducted on a CHI 760E electrochemical workstation (Chenhua, Shanghai). The CV scanning, GCD curves of PHATN-t or PHAT-t in 0.05 mM H_2SO_4 aqueous electrolyte were conducted in three-electrode system (Fig. 4d-e, Fig SX-SX), where PHATN-t or PHAT-t was used as working electrode, platinum as the counter electrode, and Ag/AgCl electrode as the reference electrode.

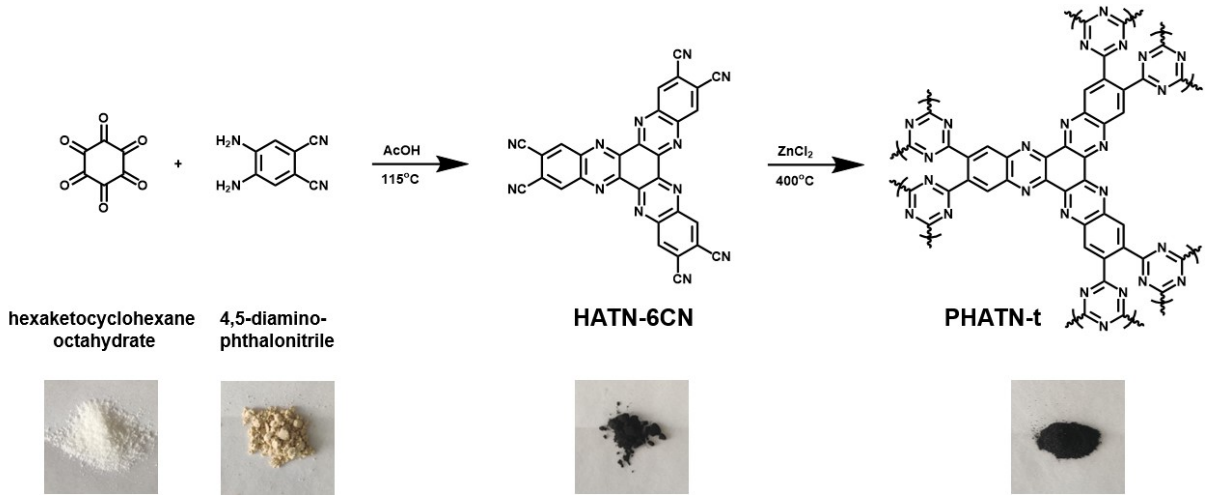

Fig. S1. The synthetic procedures of PHATN-t, together with sample photographs.

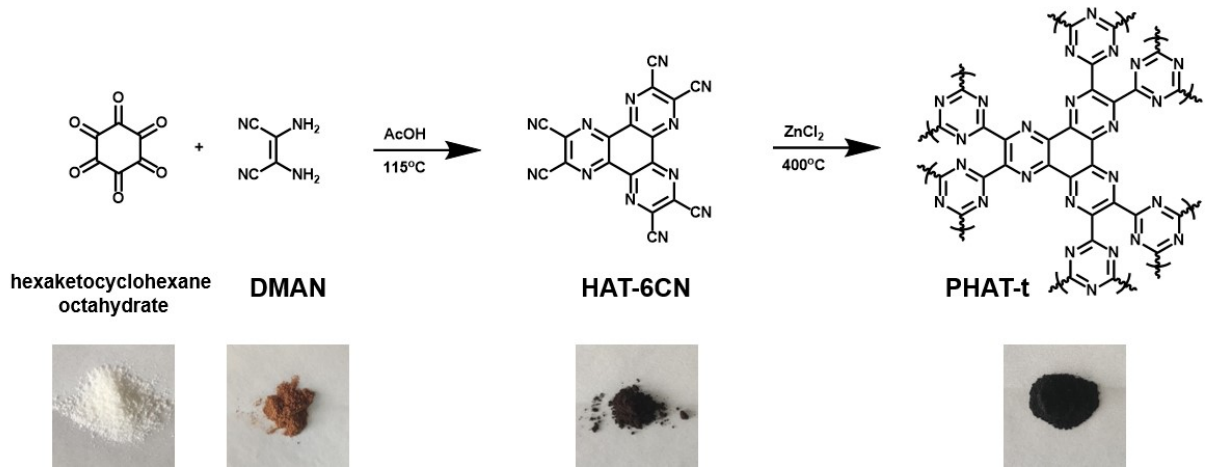

Fig. S2. The synthetic procedures of PHAT-t, together with sample photographs.

Characterization

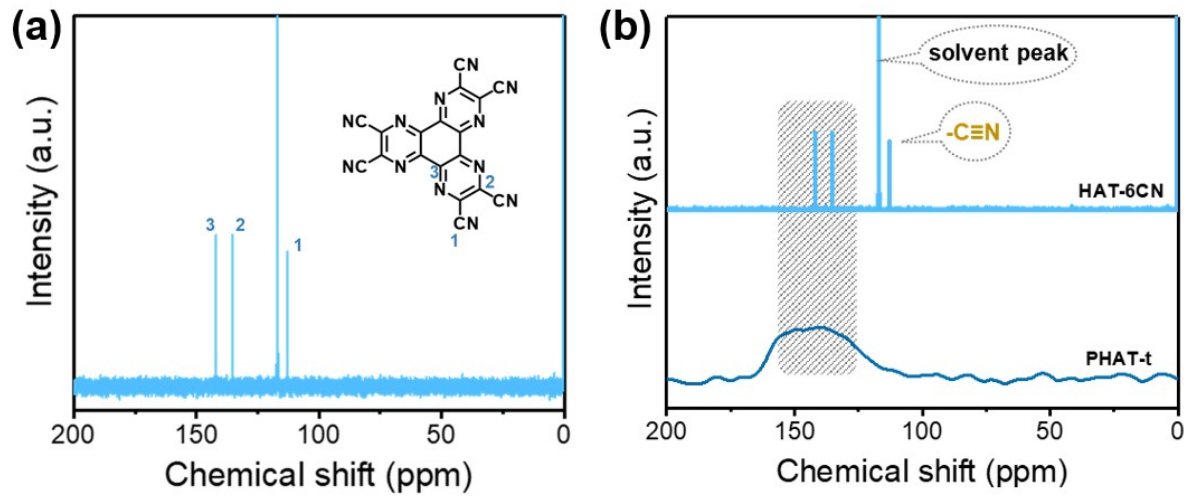

Fig. S3. (a) liquid ^{13}C NMR (CD_3CN as solvent) of HAT-6CN, and comparison with PHAT-t (solid ^{13}C NMR).

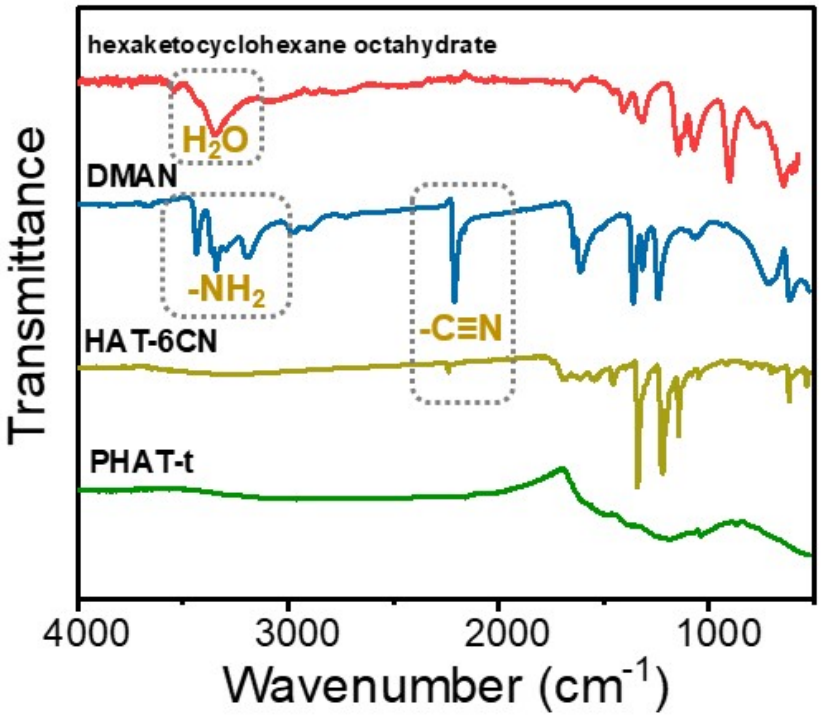

Fig. S4. FT-IR curves tracing the synthesis of PHAT-t

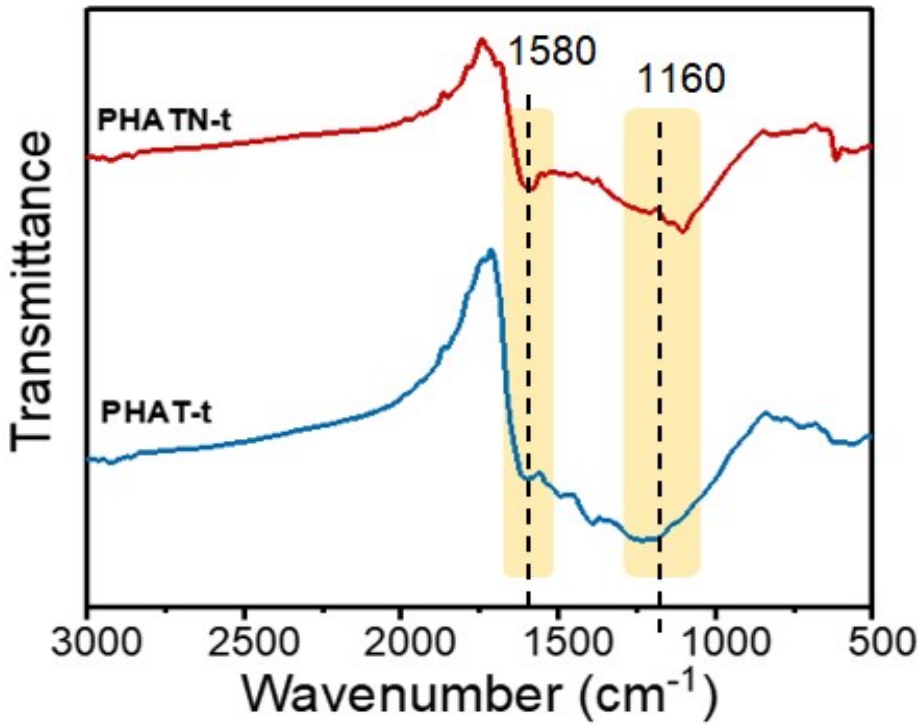

Fig. S5. The amplified FTIR curves of PHATN-t and PHAT-t for triazine rings section (yellow region).

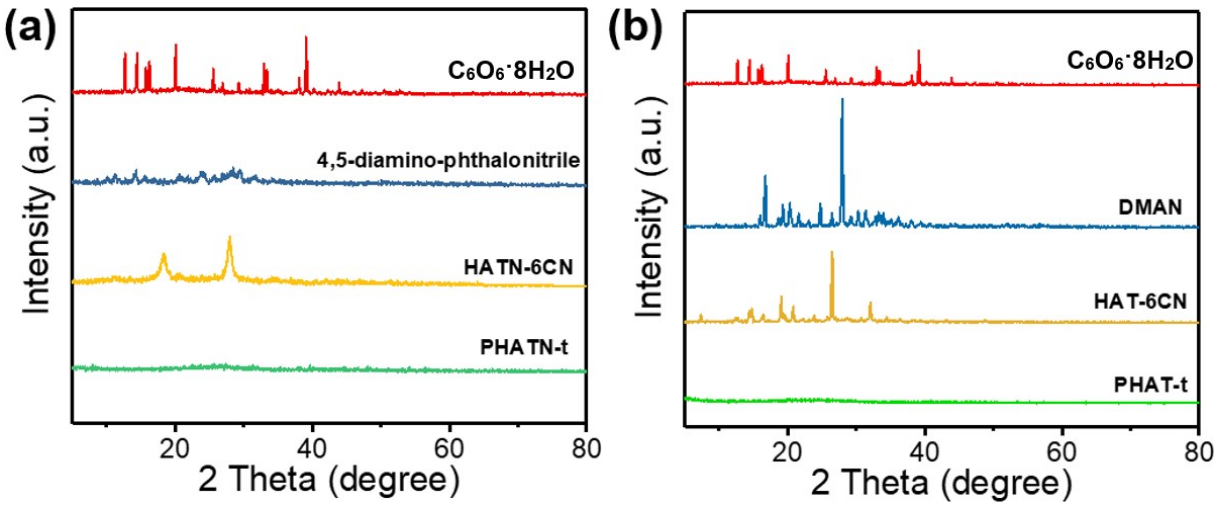

Fig. S6. XRD curves of reactants and products during synthesis process of (a) PHATN-t and (b) PHAT-t.

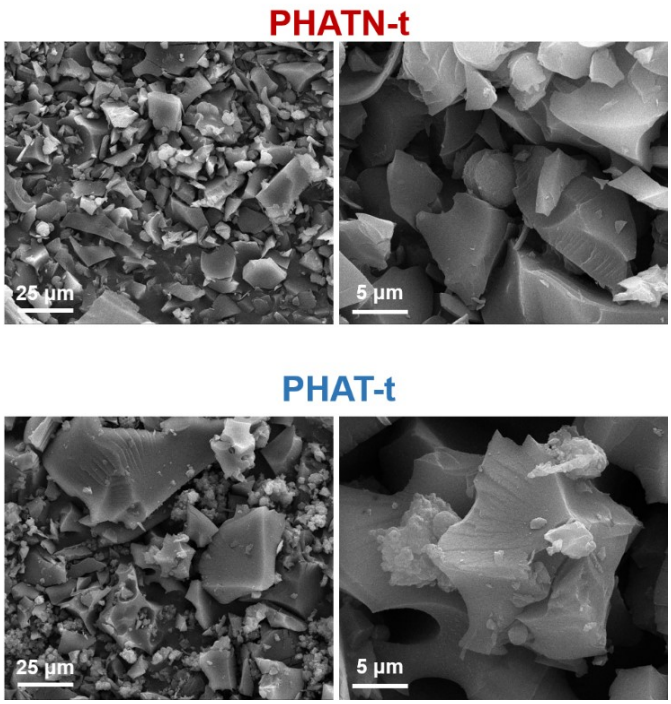

Fig. S7. SEM images of PHATN-t and PHAT-t.

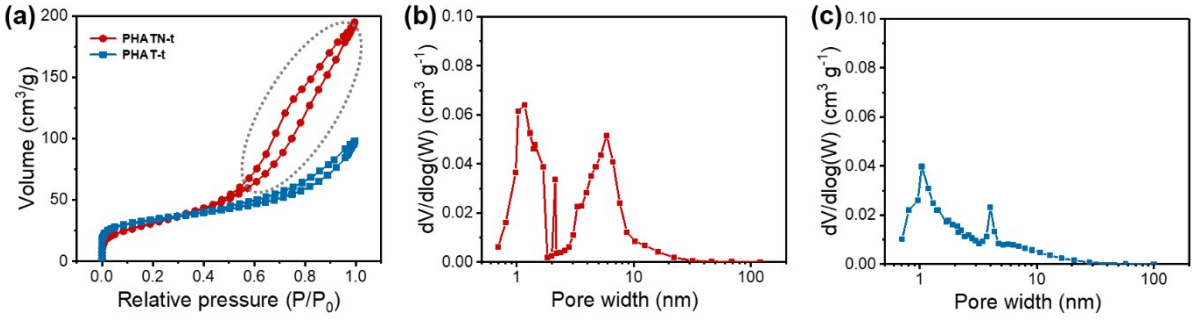

Fig. S8. (a) N_2 physisorption isotherms of PHATN-t and PHAT-t; Pore-size distribution profile of (b) PHATN-t and (c) PHAT-t.

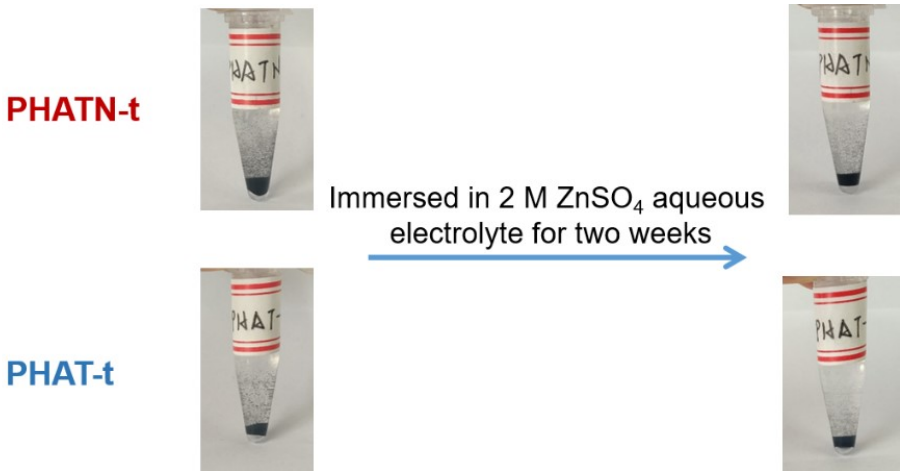

Fig. S9. Photographs of PHATN-t and PHAT-t powders before and after two weeks' immersion of 2 M $ZnSO_4$ aqueous electrolyte.

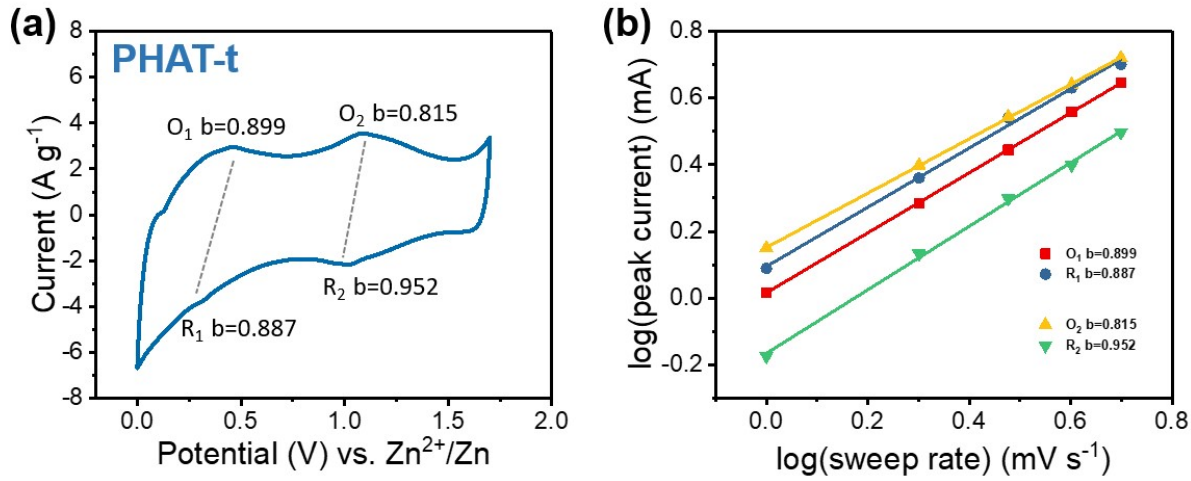

Fig. S10. (a) CV curve of PHAT-t//Zn at 5 mV s^{-1} and (b) b-value of corresponding redox peaks (O: oxidation; R: reduction).

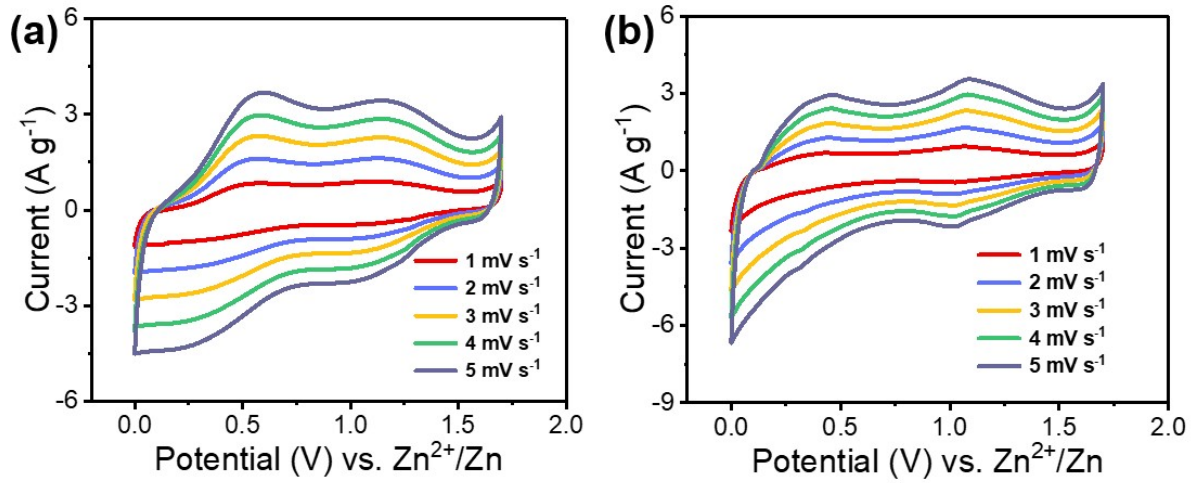

Fig. S11. CV curves of (a) PHATN-t and (b) PHAT-t against different scan rates in ZIBs.

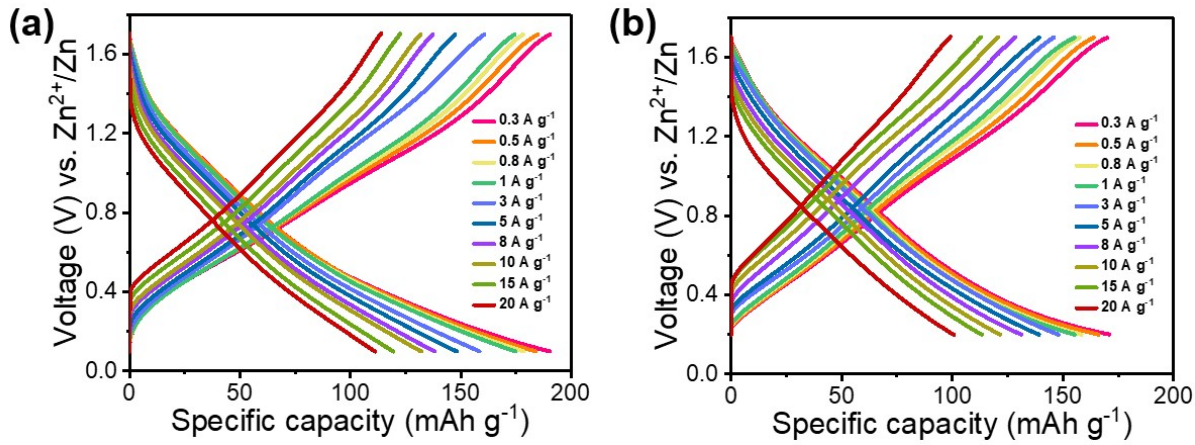

Fig. S12. GCD curves of (a) PHATN-t and (b) PHAT-t against current densities from 0.3 A g^{-1} to 20 A g^{-1} in ZIBs.

Table S1. Capacity retention comparison of PAHTN-t and PHAT-t to state-of-the-art redox polymer cathodes for ZIBs, corresponding to **Figure S12**.

Material	Electrolyte	Capacity (lowest Current density)	Retention (highest Current density)	Reference
HAQ-COF	2 M $ZnSO_4$	339 mAh g^{-1} (0.1 A g^{-1})	28% (10 A g^{-1})	S3
m-PTPA	2 M $ZnCl_2$	211 mAh g^{-1} (0.5 A g^{-1})	52% (6 A g^{-1})	S4
C@multi-layer polymer	2 M $ZnSO_4$	350 mAh g^{-1} (0.1 A g^{-1})	48% (20 A g^{-1})	S5
PDBS	2 M $ZnSO_4$	210 mAh g^{-1} (0.05 A g^{-1})	78% (5 A g^{-1})	S6
P3Q-t	2 M $ZnSO_4$	237 mAh g^{-1} (0.3 A g^{-1})	25% (20 A g^{-1})	S7
PDpBQ	2 M $ZnSO_4$	124 mAh g^{-1} (0.1 A g^{-1})	51% (5 A g^{-1})	S8
PANI-S	1 M $ZnSO_4$	180 mAh g^{-1} (0.2 A g^{-1})	75% (10 A g^{-1})	S9
PDA	3.3 M $ZnSO_4$	126 mAh g^{-1} (0.02 A g^{-1})	33% (5 A g^{-1})	S10
HqTp-COF	3 M $ZnSO_4$	200 mAh g^{-1} (0.312 A g^{-1})	62% (1.25 A g^{-1})	S11
$PoPD_H$	7.5 M $ZnCl_2$	318 mAh g^{-1} (0.05 A g^{-1})	31% (5 A g^{-1})	S12
poly(1,5-NAPD)/AC	2 M $ZnSO_4$	310 mAh g^{-1} (0.19 A g^{-1})	27% (18.5 A g^{-1})	S13
PA-COF	1 M $ZnSO_4$	265 mAh g^{-1} (0.05 A g^{-1})	25% (10 A g^{-1})	S14
PHATN-t	**2 M $ZnSO_4$**	**190 mAh g^{-1} (0.3 A g^{-1})**	**58% (20 A g^{-1})**	**This work**
PHAT-t	**2 M $ZnSO_4$**	**171 mAh g^{-1} (0.3 A g^{-1})**	**56% (20 A g^{-1})**	**This work**

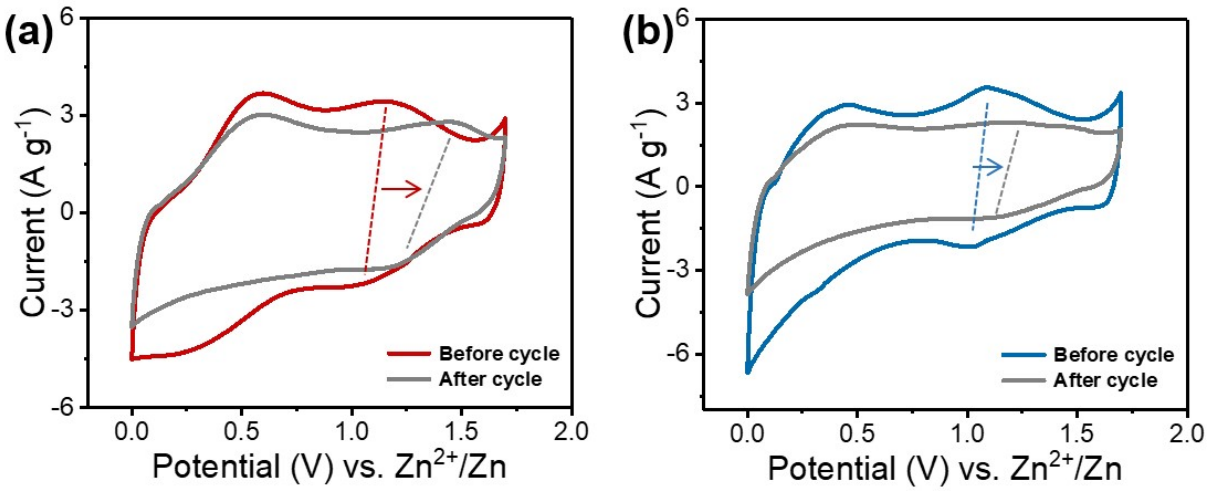

Fig. S13. CV curves of (a) PHATN-t and (b) PHAT-t at 5 mV s^{-1} before and after GCD cycles.

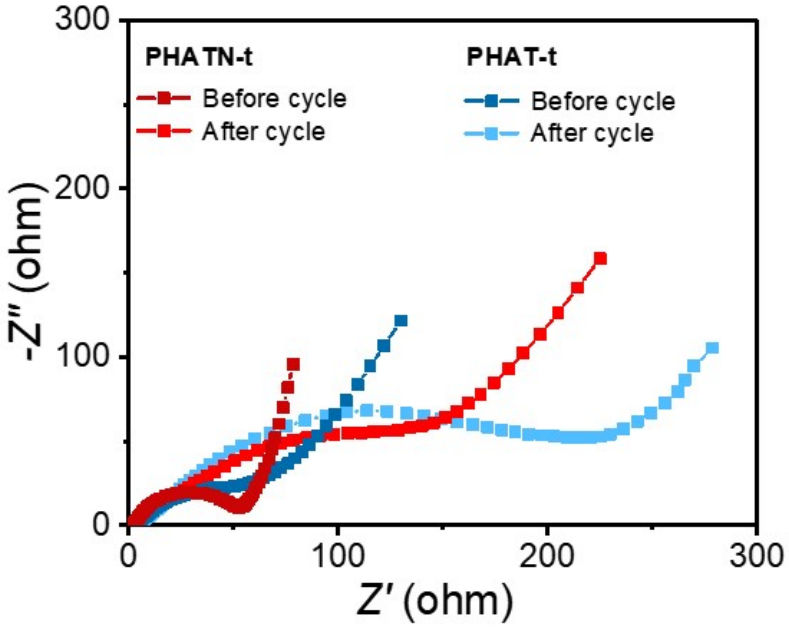

Fig. S14. EIS of PHATN-t and PHAT-t collected before and after 1000 GCD cycles.

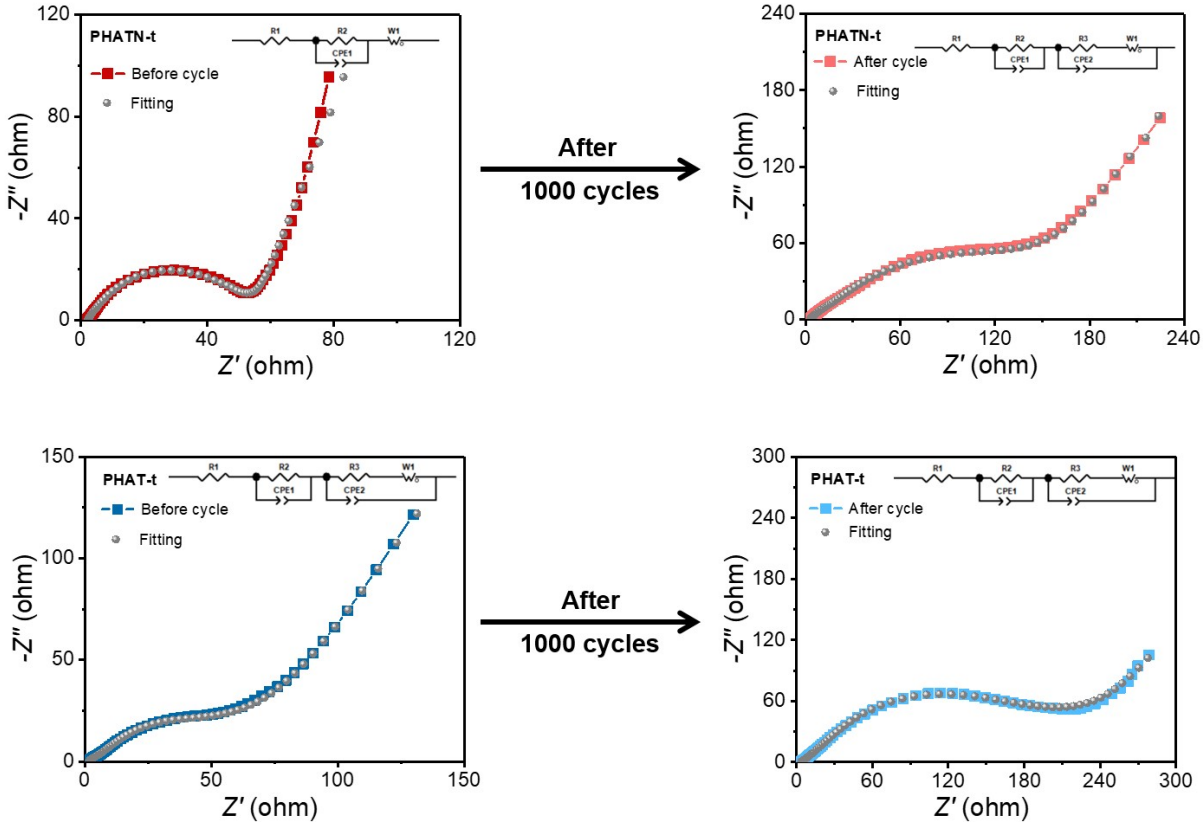

Fig. S15. EIS fitting of PHATN-t and PHAT-t collected before and after GCD cycles.

Table S2. The EIS fitting results of PHATN-t and PHAT-t collected before and after 1000 GCD cycles.

Sample	State	R_1	R_2	R_3	CPE_1-T	CPE_1-P	W_1-R	W_1-T	W_1-P	CPE_2-T	CPE_2-P
PHATN-t	Pristine	2.08	48	——	1.39×10^{-3}	0.80	15	1.58	0.41	——	——
	1000th	2.86	136	12.63	3.21×10^{-3}	0.68	957	168.90	0.69	2.07×10^{-3}	0.67
PHAT-t	Pristine	1.67	23.24	5.01×10^{-7}	4.35×10^{-3}	0.84	133	15.51	0.34	3.1×10^{-5}	0.99
	1000th	3.34	91.72	197	1.51×10^{-3}	0.87	54	4.63	0.37	4.8×10^{-5}	0.43

Notes: The series resistance (R_1) includes the resistance of the electrolyte, separator and electrode materials. R_2 and R_3 represents the charge transfer resistance (Rct) that is associated with the semicircle at high-frequency region.

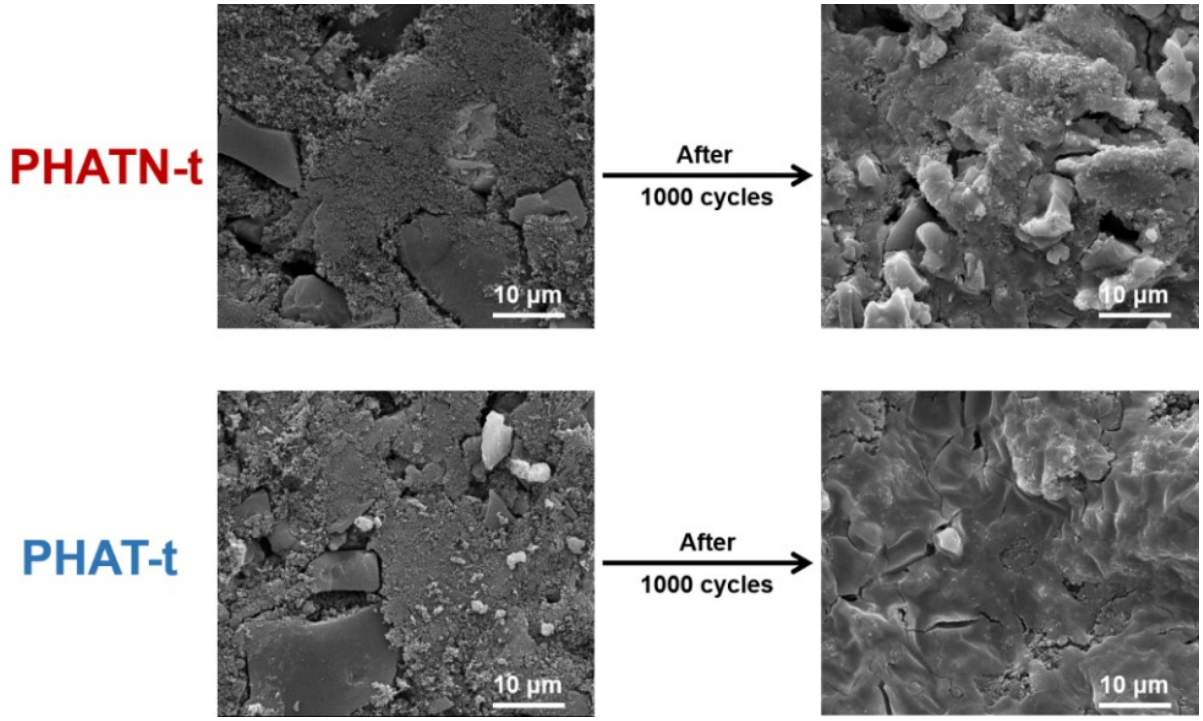

Fig. S16. SEM images of PHATN-t and PHAT-t in ZIBs before and after GCD cycles.

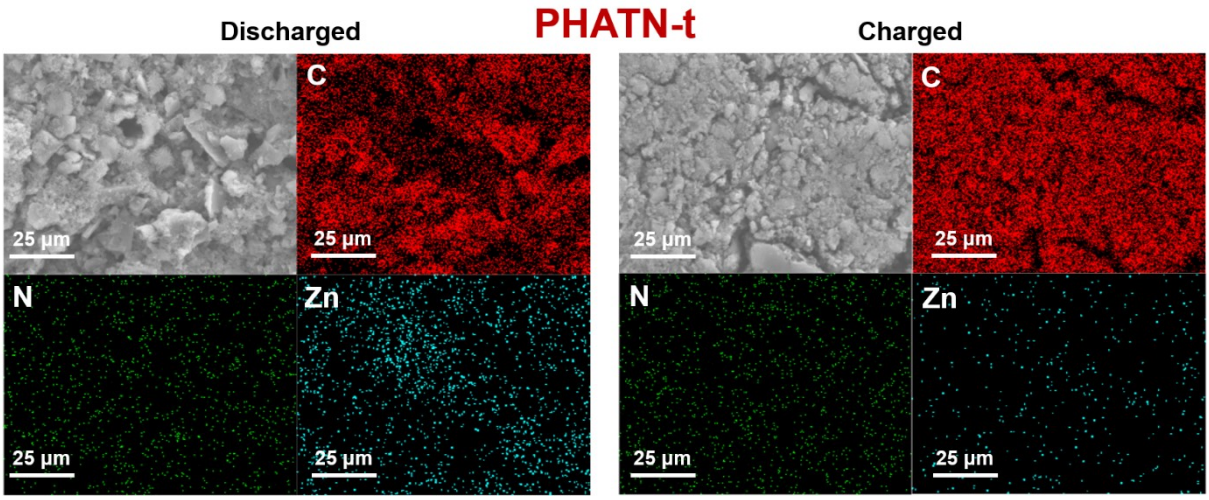

Fig. S17. Corresponding element energy-dispersive spectroscopy (EDS) mapping of PHATN-t at discharged (0.1 V) and charged (1.7 V) state in ZIBs.

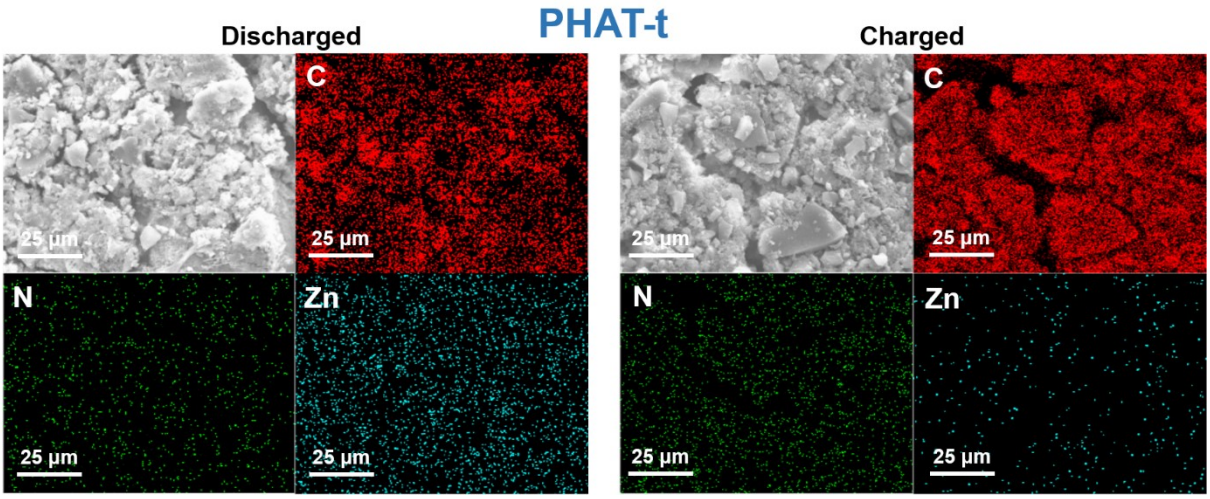

Fig. S18. Corresponding element energy-dispersive spectroscopy (EDS) mapping of PHAT-t at discharged (0.1 V) and charged (1.7 V) state in ZIBs.

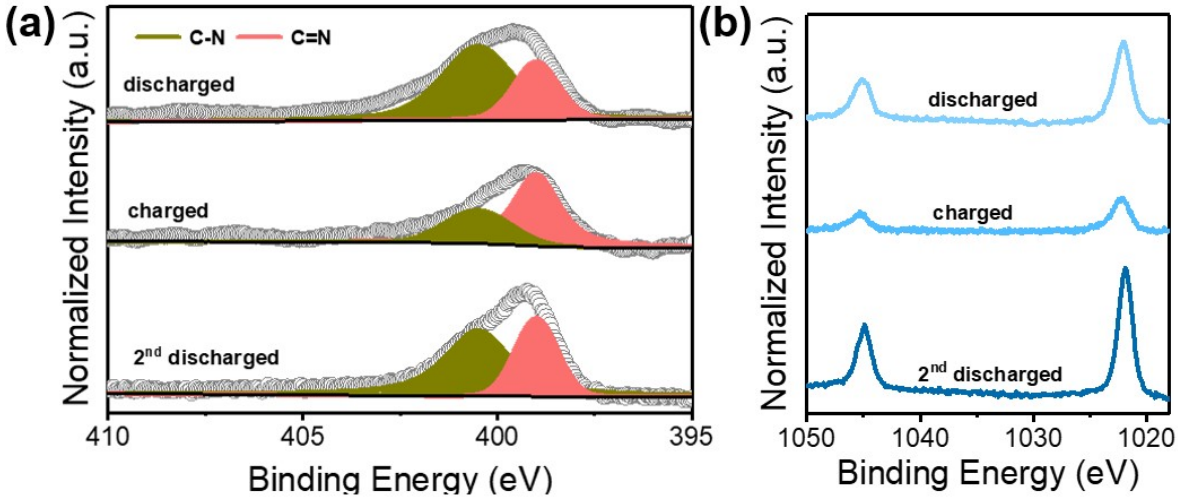

Fig. S19. (b) N 1s regions and (c) Zn 2p region of high-resolution of PHAT-t at different states.

Table S3. The C-N/C=N ratio of PHATN-t and PHAT-t at charged/2nd discharged state.

Element	PHATN-t		PHAT-t	
	charged	2nd discharged	charged	2nd discharged
C-N	38.4%	69.7%	40.9%	64.4%
C=N	61.6%	30.3%	59.1%	35.6%
Zn^{2+} migration	50.3%		79.2%	

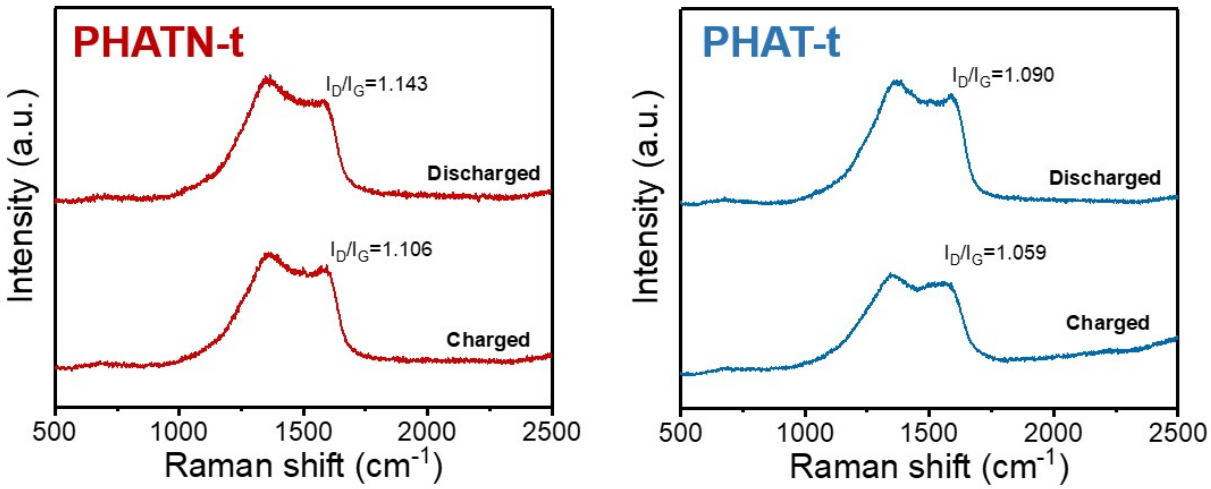

Fig. S20. Raman curves of PHATN-t and PHAT-t at discharged (0.1 V) and charged (1.7 V) state in ZIBs.

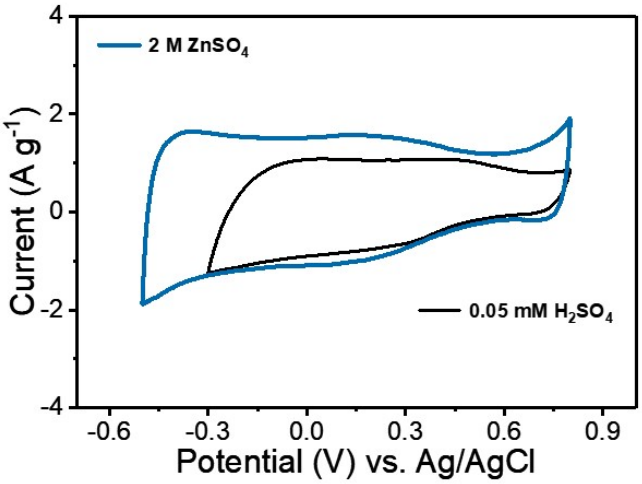

Fig. S21. PHAT-t in 2 M ZnSO4 and 0.05 mM H_2SO_4 aqueous electrolytes at scan rate of 5 mV s^{-1} in three-electrode system.

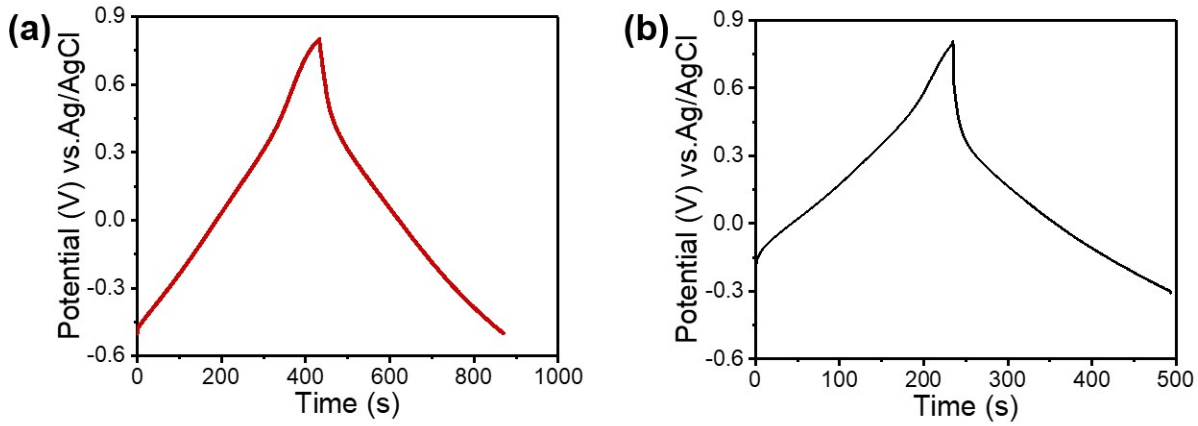

Fig. S22. GCD curves (1 A g^{-1}) of PHATN-t in (a) 2 M $ZnSO_4$ and (b) 0.05 mM H_2SO_4 conducted by three-electrode system.

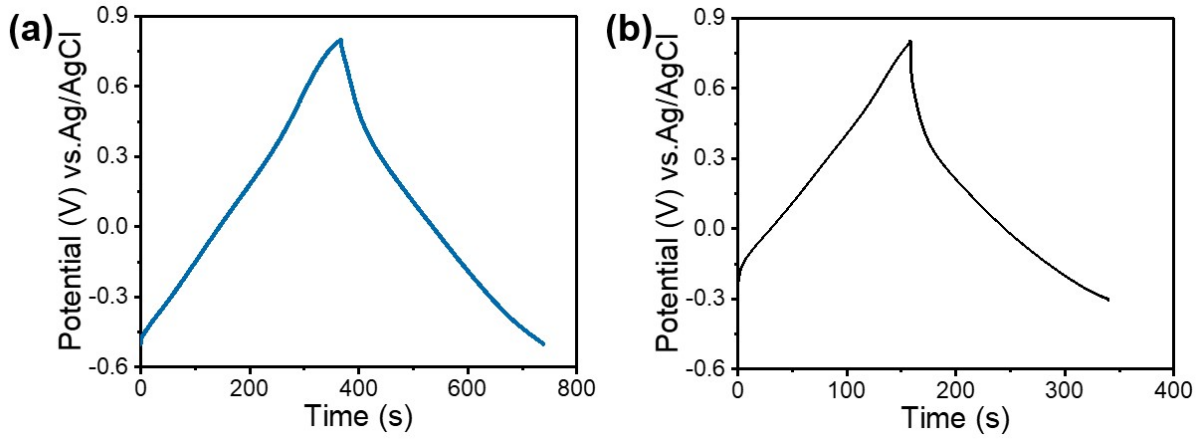

Fig. S23. GCD curves (1 A g^{-1}) of PHAT-t in (a) 2 M $ZnSO_4$ and (b) 0.05 mM H_2SO_4 conducted by three-electrode system.

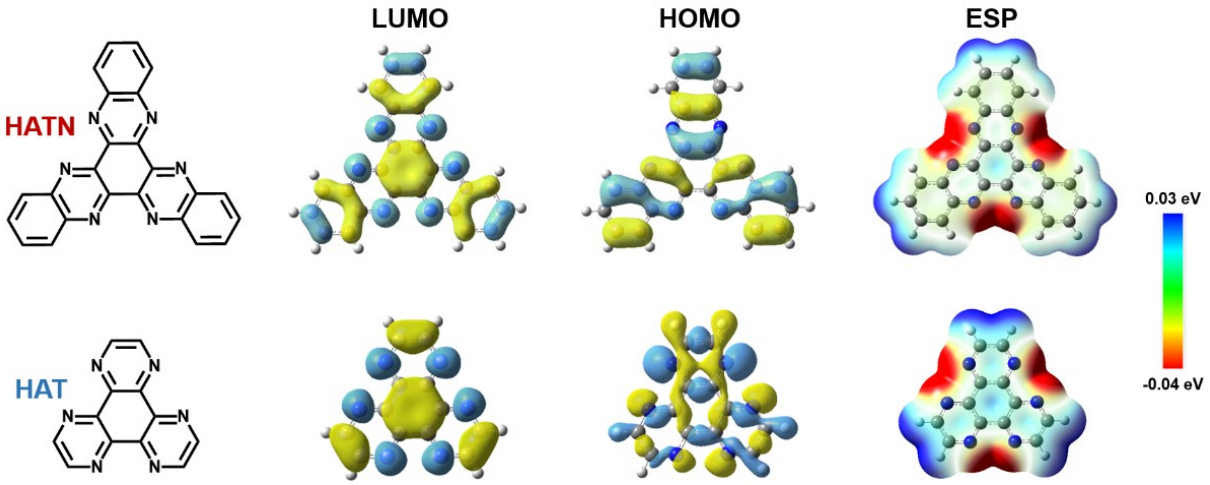

Fig. S24. DFT-optimized LUMOs and HOMOs of HATN and HAT, as well as corresponding ESP profiles.

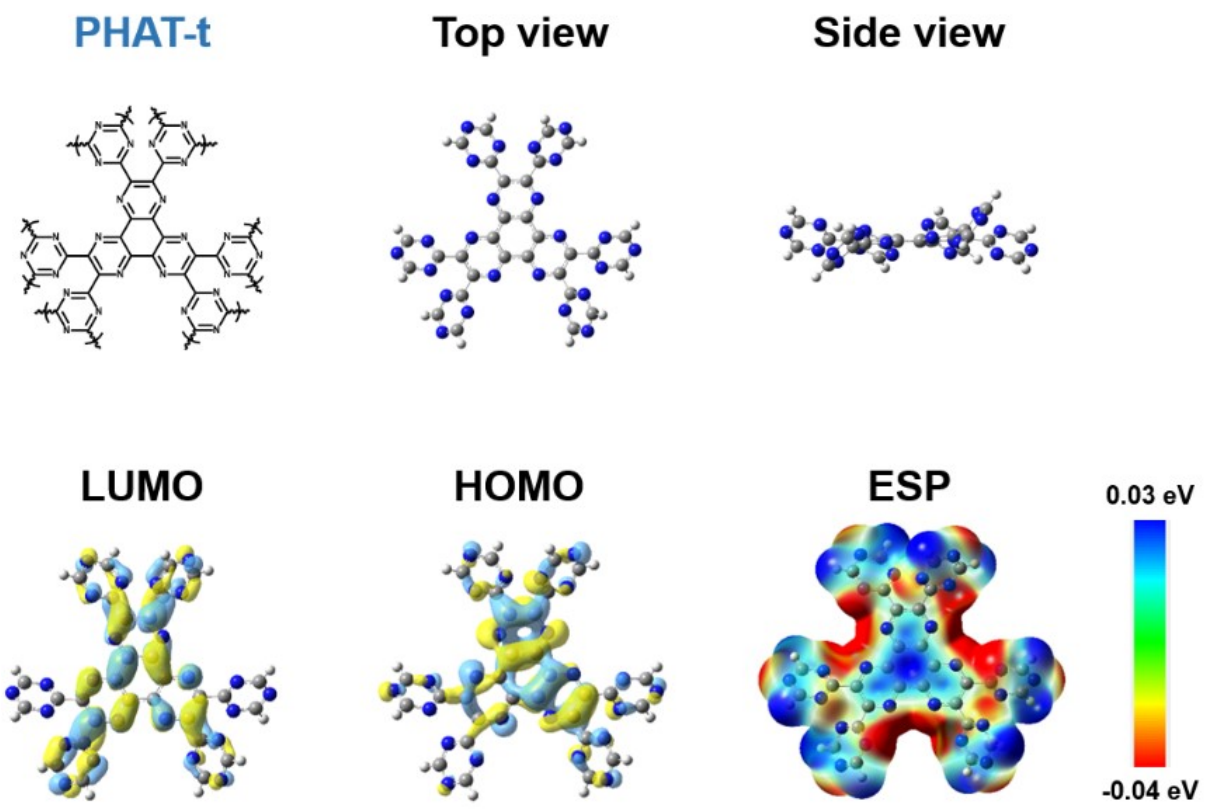

Fig. S25. DFT-optimized geometries, LUMOs and HOMOs of PHAT-t, as well as corresponding ESP profiles.

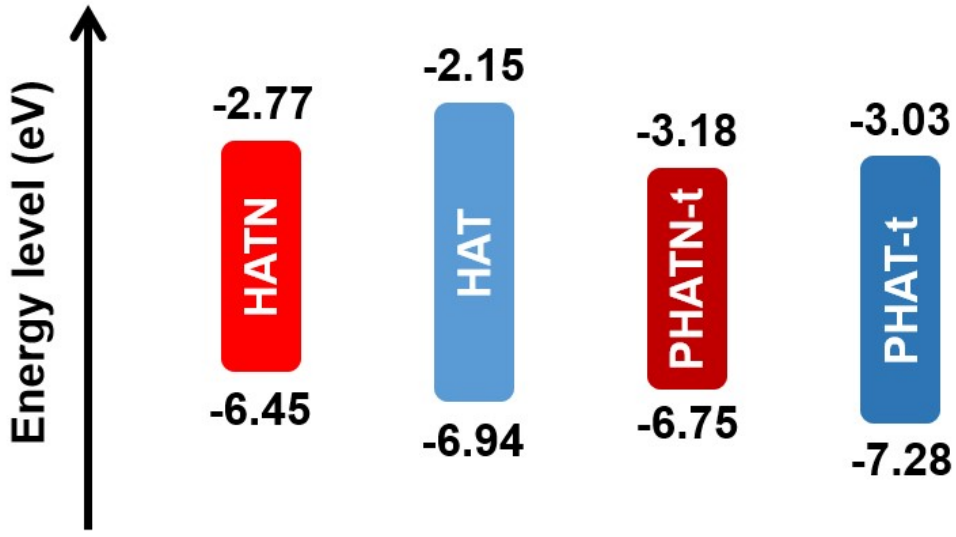

Fig. S26. DFT-optimized energy level gaps of HATN, HAT, PAHTN-t and PHAT-t.